Biocomposites of poly (lactic acid) and lactic acid oligomer - grafted bacterial cellulose: It's preparation and characterization

Rahul Patwa[1], Nabanita Saha[2*], Petr Sáha[2] and Vimal Katiyar[1*]

[1]Department of Chemical Engineering, Indian Institute of Technology Guwahati, Guwahati, Assam, India-781039

[2]Centre of Polymer Systems, University Institute, Tomas Bata University in Zlín, Tř. T. Bati 5678, 760 01 Zlín, Czech Republic

[*]Corresponding author, Email: vkatiyar@iitg.ac.in, nabanita@utb.cz

Abstract

This work demonstrates the synthesis of lactic acid oligomer-grafted-untreated bacterial cellulose (OLLA-g-BC) by insitu condensation polymerization which increased compatibilization between hydrophobic poly (lactic acid) PLA and hydrophilic BC, thus enhancing various properties of PLA-based bionanocomposites, indispensable for stringent food-packaging applications. Infrared spectroscopy confirms the grafting of OLLA-chains onto BC backbone through hydroxyl groups. Homogeneous dispersion of BC nanospheres can be seen in bionanocomposites using Transmission-microscopy. Bionanocomposites displayed comparable tensile strength but elongation showed ~20% improvement with 20wt% addition. The maximum degradation for PLA/OLLA-g-BC bionanocomposites was comparable to PLA and above the PLA processing temperature indicating that bionanocomposite processing can be industrially-viable. The glass transition (T_g) showed a decrease upon addition of fillers indicating towards plasticization of PLA which is highly required for flexible-food packaging. The crystallization and POM studies revealed that fillers can enhance the crystallization rate at higher concentrations and spherulitic growth improved significantly. The transparency of films showed slight reduction but act as excellent UV-blocking agents. The prepared bionanocomposites were hydrophobic with contact angle of 102.5°. The water-vapor barrier for bionanocomposites was improved ~40% by 5% addition, which is significant. The reduced T_g, improved elongation combined, improved hydrophobicity and water-vapor barrier make them suitable for flexible food-packaging applications.

Keywords: Bacterial cellulose, poly (lactic acid), insitu polymerization, bionanocomposites

Introduction

Depleting fossil reserves and the environmental concerns arising due to its continuous use for production petroleum-based polymers have pushed the scientific community to look for alternative bioplastics which are obtained from renewable sources. Currently, many biopolymers are available such as polycaprolactone (PCL), polyhydroxyalkanoates (PHA), polybutylene succinate (PBS), polyglycolic acid (PGA) and poly(lactic acid) (PLA), etc. Out of all of the available biopolymers available in the market, PLA has emerged as the most widely researched bio-based plastic [1,2]. PLA is a thermoplastic aliphatic polyester which uses lactic acid (2-hydroxy propionic acid) obtained upon fermentation of sugars derived from natural resources such as sugar beet, sweet potato, corn, etc [3,4]. It has many unique features such as it is bio-compostability, biocompatibility, hydrophobic nature, non-toxicity and melt-processability [5-9]. PLA possesses certain limitations such as low melt stability, brittleness, high permeation to gas and water compared to other commercial plastics used for food packaging. For PLA to be able to replace conventional packaging plastics extensive improvement in its barrier and thermomechanical properties is required. To achieve material properties comparable to other benchmark packaging plastics various strategies are devised such as stereo-complexation, blending, addition of nano- and micro-fillers, etc [10-12]. Reinforcement of PLA matrix by addition of fillers such as cellulose nanocrystals, chitosan, gum, hydroxyapatite, silk, etc can be used to form bionanocomposites with the desired properties for packaging [10,13-16]. Superiority of filler reinforced polymer bionanocomposites is dictated by dispersion and interfacial adhesion. Therefore, dispersion of filler particles inside the polymer matrix becomes a key factor for nanocomposite properties [12,17]. The filler dispersion can be improved by numerous techniques such as grafting, sonication, compounding, insitu polymerization [17-20]. In situ polymerization approach has been widely used for dispersion of fillers such as chitosan, gum, clay, etc into the PLA matrix to prepare 'green biocomposites' with potential to become future fabrication materials [1,3,15].

Bacterial cellulose (BC) is polysachharide produced by several species of bacteria such as *aoetobacter pasterianus, gluconacetobacter xylinus, acetobacter hansenii,* etc as an extracellular protective coating [21,22]. Unlike plant cellulose BC is pure cellulose without lignin where two cellobiose units are arranged in parallel conformation. It is composed of random arrangement of cellulose microfibrils of ~100 Å diameter [23]. Bacterial cellulose has superior mechanical properties due to its better arrangement of fibers which results in higher crystallinity. To utilize its properties BC has been utilized in a variety of polymers as a reinforcement viz. polyaniline (PANi), polyvinyl alcohol (PVA), polycaprolactone. etc [24-26]. It

is noteworthy to mention that BC are hydrophilic in nature which limits its dispersion into the hydrophobic polymer matrix ultimately affecting the interfacial adhesion between BC and polymer thus severely affecting the overall properties of the biocomposites [27] In order to achieve a better dispersion of BC, a masterbatch (MB) of OLLA-g-BC was obtained upon in situ condensation polymerization reaction of lactic acid solution pre-incorporated with bacterial cellulose. PLA and OLLA-g-BC are used to prepare composite films by film cast method where PLA and OLLA-g-BC are matrix and filler materials, respectively. Different proportions of PLA and OLLA-g-BC are used and the prepared bionanocomposite films are termed as PLA/OLLA-g-BC and evaluated for physico-chemical, thermal, surface and mechanical properties.

Experimental methodology

Materials

PLA granules (grade: 2003D, D-lactic acid: 98.6%, density: 1.24 Kg/m^3) was supplied by NatureWorks® LLC, Minnetonka, MN, U.S.A. having number (M_n) and weight (M_w) averaged molecular weights of ~150 kDa and ~200kDa, respectively. Bacterial cellulose (BC) used in this study was produced by bacterial strain procured from Czech Collection of Microorganisms (CCM), Brno, Czech Republic. L-lactic acid (~90 wt% was supplied by Purac, India. Solvents such as acetone were supplied by Fisher Scientific, India. De-ionized water was synthesized from Milli-Q synthesis unit, Millipore® (TOC<10ppb; particles<0.22μ/ml and resistivity: ~18.2MΩ.cm at 25°C). HPLC grade chloroform was procured from Merck, India. All chemicals were used as supplied without any purification.

Lactic acid oligomer-untreated bacterial cellulose masterbatch (MB) synthesis

Untreated bacterial cellulose solution (pH=3) and lactic acid were added in the ratio of 50:50 (v/v) and mixed using high speed homogenizer (IKA, India) at ~25000 rpm for 1 minute. This mixture was kept in a three-necked round flask dipped in silicone oil bath maintained at 120 °C under inert atmosphere maintained by argon flow. The reaction setup as shown in Figure 1 was equipped with a hot plate cum magnetic stirrer supplied with a temperature probe, recirculating chiller, fiberglass heating tape and vaccum system through a cold trap. The mixture was initially stirred at ~250 rpm for 2h at room temperature. Later temperature was ramped to 150 °C and applied pressure was ~100 mmHg for 2h finally the pressure was reduced to ~30 mmHg using standard vacuum pump and reaction was continued for 4h. The final

product obtained a viscous dark brown consistency where BC was within the oligomers of lactic acid. This was used as a reinforcement filler to prepare PLA/OLLA-g-BC solution cast films.

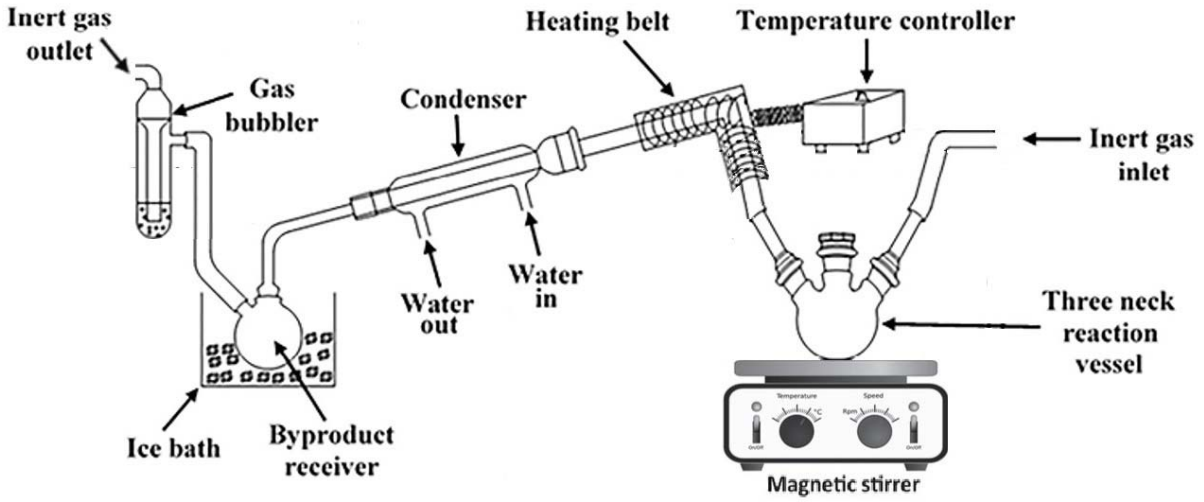

Figure1: Experimental setup for synthesis of OLLA-g-BC masterbatch (MB).

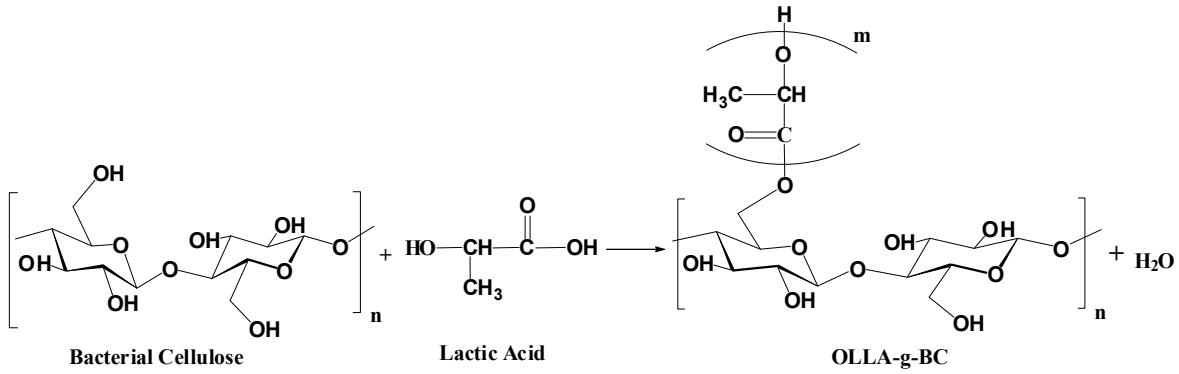

Scheme 1. Schematic representation of the synthesis of OLLA-g-BC.

Preparation of films

In this work, films of PLA and PLA containing MB in different proportions viz. 5.0, 10.0, 20.0 and 30.0%, respectively and are labelled as PLA/OLLA-g-BC (5%), PLA/OLLA-g -BC (10%), PLA/OLLA-g-BC (20%) and PLA/OLLA-g-BC (30%), respectively. The bionanocomposite

films were fabricated by solvent casting method and solvent used in this study was chloroform. Calculated amounts of PLA granules and OLLA-g-BC masterbatch were added to round bottom flask containing chloroform stirring at ~500 rpm, the contents were allowed to stir overnight and were cast on Teflon petridishes and solvent was allowed to dry. Once the solvent is dried up the films are carefully peeled off and kept in vacuum oven (40 °C, 12h) for complete removal of solvent and inbound moisture. Once the films are dried they are kept in ziploc bags and stored in desiccator until further use.

Analytical instrumentation and characterization

Fourier transformed infrared spectroscopy (FTIR)

To difference in chemical structures of PLA and bionanocomposites films were determined using a Frontier-1 FTIR spectrometer (PerkinElmer, USA) attached with an attenuated total reflectance mode (ATR) assembly. Scans were carried out with 4.0 cm^{-1} resolution and 64 scans over 650-4000 cm^{-1} wavenumber range. Before analysing, the film samples were vacuum dried overnight at 50 °C, to remove the trace amounts of moisture.

Gel permeation chromatography (GPC)

Molecular weights of all formulations was estimated using the LC-20A GPC (Shimadzu, Japan) fitted with two 5µm PLgel columns and used HPLC chloroform as eluent (1 mL/min, 40 °C). Measured quantities (~40mg) of samples were dissolved in HPLC grade chloroform (~1.5 mL) and were filtered using 0.2 µm PTFE filters.

Surface morphology

The cross-sectional surface morphology of cryofractured film samples was studied using a Sigma, field emission scanning electron microscope (FESEM) (Zeiss, USA). Prior to analysis the sample was coated with gold by plasma sputtering (SC7620, Quorum) under vacuum for 120s. Operating voltage and working distance were set between 2 to 3 kV and 5 mm, respectively. The cryofractured cross-sections of films were mounted onto aluminium stubs by using double-sided carbon tapes. To observe the bulk morphology and nano level dispersion of untreated BC inside the PLA/OLLA-g-BC bionanocomposite films a JEM-2100 transmission electron microscope (JEOL, USA) was used. A small piece of bionanocomposite film was dissolved in HPLC grade chloroform and vortexed for 1 minute. Subsequently, one

drop of solution was cast on carbon-coated TEM grid (PacificGrid, USA) and vacuum dried overnight at 50 °C.

Differential scanning calorimetry

Thermal properties of PLA and bionanocomposite films was examined using DSC 204F1 differential scanning calorimeter (DSC) (Netzch, Germany). Sample (8.0±0.5 mg) was kept in platinum crucible under nitrogen flow of 20mL/min and heated from 25 °C to 190 °C at a rate of 10 °C/min followed by a 3 min isothermal hold in order to remove any thermal history after which the sample was cooled to 25 °C at a rate of 10 °C/min and finally the sample was again heated to 190 °C at 10 °C/min rate. Thermal data such as glass transition temperature (T_g), cold crystallization temperature (T_{cc}), enthalpy of crystallization (ΔH_{cc}), melting temperature (T_m), enthalpy of fusion (ΔH_m) and percentage crystallinity ($\%X_c$) from the second heating cycle were reported. The percentage crystallinity was calculated as per Equation 1.[12]

$$\%X_c = \frac{\frac{\Delta H_m - \Delta H_{cc}}{\Delta H_m^{\circ}}}{93.7\left(1-\frac{\%wt\ of\ filler}{100}\right)} \times 100 \quad (1)$$

In order to study the kinetics of isothermal crystallization, the samples were heated from ambient temperature to 190 °C at a rate of 10 °C/min after which a 3 min isothermal hold was given to erase thermal history. Subsequently, the sample was flash cooled to 120 °C at °60 C/min and held isothermally for 1 hour for complete crystallization to occur. Thereafter, the sample was allowed to cool back to room temperature.

Isothermal crystallization kinetics theory

To evaluate the effect of OLLA-g-BC fillers on the crystallization process, relative crystallization (X_t) with respect to time can be calculated according to the Equation 2.[28]

$$X_t = \frac{\Delta H_t}{\Delta H_\infty} = \frac{\int_0^t \left(\frac{dH}{dt}\right).dt}{\int_0^{t\infty} \left(\frac{dH}{dt}\right).dt} \quad (2)$$

where, ΔH_t, ΔH_∞ and $\frac{dH}{dt}$ are enthalpies at any time t, at complete crystallization and heat evolution rate, respectively. Furthermore, Avrami theory (Equaltion 3) is applied for understanding the isothermal crystallization behaviour of PLA and bionanocomposite films.[28] The main assumption of this theory is that relative crystallinity increases with increase in crystallization time.

$$1 - X_t = exp(-Kt^n) \quad (3)$$

This logarithmic form of the above equation is as follows[28]:

$$ln[-ln(1 - X_t)] = \ln K + n \ln t \quad (4)$$

where, X_t, t, K and n are the relative crystallinity term, crystallization period, rate of crystallization constant and Avrami exponent, respectively. Avrami exponent (n) gives an idea about the type of nucleation and hence the mechanism whereas the constant (K) gives information about growth rate parameters. The slope and intercept from the ln[-ln(1-X_t)] vs. ln t plots gives n and K, respectively. The secondary crsytallization i.e the non-linear portion of the relative crystallization plots is ignored and only the linear portion (Xt=30-70%) which is the primary crystallization is considered for the crystallization kinetic studies. Crystallization half-time is a very important parameter which is the time required for half crystallization of the sample. It can be calculated using Equation 5.[28]

$$t_{0.5} = \left(\frac{\ln 2}{K}\right)^{0.5} \quad (5)$$

The $t_{0.5}$ value can be used to predict the rate of crystallization.

Polarized optical microscopy (POM)

The growth rate of spherulites was measured using an Eclipse LV100N POL polarized optical microscope (Nikon, Japan) equipped with a TST350 sample heating stage (Linkam, UK). The samples were heated from room temperature to 190 °C and isothermally held to erase any thermal history. Later, the sample was rapidly cooled to 120 °C at a rate of 60 °C/min and held for 30 min. The spherulite morphology was recorded using the CCD camera attached with the POM and the spherulitic growth rate (G) was estimated from the slope of spherulitic radius (R)-crystallization time (t) plots as per the Equation 6.[28]

$$G = \frac{dR}{dt} \quad (6)$$

Thermogravimetric analysis (TGA)

Thermogravimetric analysis of the prepared films (8.0±0.5 mg) was done using a TGA4000 thermogravimetric analyser (PerkinElmer, USA). The thermographs were obtained by placing the sample in an aluminium crucible and heating from room temperature to 700 °C at 5 °C/min under inert gas flow of 20 ml/min.

Mechanical properties

Mechanical property characterization of the formulations such as tensile strength, Young's Modulus, percentage elongation at break, etc. were determined using the KIC-050-C universal tensile testing machine (Kalpak Instruments, Pune, India). for mechanical testing, the film samples were cut into strips of dimensions 60×5×0.4 mm as per ASTM D882-12, the crosshead speed was set to 5 mm./min.

Dynamic mechanical analysis

Thermomechanical information about the formulations such as storage modulus ($E^{'}$) and loss factor (tan δ) were estimated using DMA242 (Netzsch, Germany) dynamic mechanical analyser (DMA). The specimens (10 × 5 × 2 mm^3) were heated from 25 to 90 °C at a ramp of 3 °$Cmin^{-1}$ in tensile mode under nitrogen flow (100 $mLmin^{-1}$) and operating frequency, force and deformation distance were kept at 1 Hz, 2 N and 0.04 mm, respectively.

Contact angle analysis

Surface wettability in form of contact angle was measured using the DSA-25 goniometer (Krüss, Germany). Contact angles of PLA and bionanocomposite films were determined using the sessile drop method where deionized water drop (~2 µl) was used. The contact angles were measured exactly after a minute of releasing the drop on the film surface in order to stabilize the drop. The formation of drop on the film surface was captured using the CCD camera. The analysis was performed in triplicates at 23 °C and mean with standard deviation are reported.

Water vapor transmission rate (WVTR)

Water vapor transmission rates (WVTR) was determined using the Permatran-W® 1/50G water vapour permeability tester (Mocon, USA) according to the ASTM E398-03. The films each of 50 cm^3 were conditioned at 38±2 °C for 48h prior to analysis. The analysis was performed in triplicates at 37.8±0.1 °C and 90 % RH under nitrogen flow (30-35 psig, 99.99% purity). The samples were exposed until three consecutive readings displayed only a 5% deviation and was considered as the WVTR of that particular formulation. (~99.999% purity). Water permeability values were calculated from WVTR values using the following Equation 7.

$$WVP = \frac{WVTR \times t}{\Delta P} \quad (7)$$

where, WVTR values are obtained in gm/m^2.day, t denotes the thickness of films in mm and ΔP is the partial pressure difference between the two sides of the film placed in test chamber.

Optical Studies

Opacity of bionanocomposite films prepared using all formulations was studied using a Lambda 35 UV-visible spectrophotometer (PerkinElmer, USA). The range, rate and spectral width were set to 190-1100 nm, 50 nm/min and 2 nm, respectively. The opacity is calculated as average of three values using the following equation 8:

$$Opacity = \frac{A_{600}}{t} \quad (8)$$

where, A_{600} is the absorbance at 600 nm and t denotes the film thickness (mm).

Psychometric or chroma co-ordinates (L^*, a^* and b^*) for different film formulations were obtained using a series 550 chromameter (Datacolor, USA) as per the ISO 9001:2008 standard. Calibration was carried out using the white calibration tile with the following CIE values lightness(0)/darkness(100), L^*= 89.35; redness (+ve)/greenness (-ve), a^* = -0.22 and yellowness (+ve)/blueness (-ve), b^*= +4.79. Total color difference (ΔE^*) between films prepared from different formulations and standard was calculated using the following equation 9:

$$\Delta E^* = \sqrt{(\Delta L^*)^2+(\Delta a^*)^2+(\Delta b^*)^2} \quad (9)$$

Similarly, Chroma (C^*) value which gives information about the color saturation was also determined by using the following Equation 10.

$$C^* = \sqrt{(\Delta a^*)^2+(\Delta b^*)^2} \quad (10)$$

Results and discussions

FTIR studies

The infrared spectrum of PLA and PLA/OLLA-g-BC film bionanocomposites with varying concentration of OLLA-g-BC were obtained and shown in Figure 2. PLA films show characteristic absorptions bands at 754, 869, 1083, 1182, 1352, 1382, 1454 and 1747 cm^{-1} which ascribe to –CH– bending, –C–C– stretch, –C–O– stretching, $–CH_3$ angular deformation, –CH deformation, $–CH_3$ bending and –C=O stretching, respectively.[3,29] The OLLA-g-BC shows the formation of PLA chains during the insitu melt polycondensation due to the presence

of strong band at 1755 cm^{-1} which ascribes to the carbonyl stretching (C=O)[3] Peaks at 1456, 1188 and 1092 cm^{-1} are observed which represent the stretching, rocking and assymetric vibrations, repectively of the –C–CH_3 in polylactide.[17] It is noteworthy to mention that the peaks present in the region 3400-3500 cm^{-1} which ascribe to –OH groups of bacterial cellulose are now missing in the OLLA-g-BC. This could be due to the interaction of –OH polar groups during polymerization. The MB shows weak bands at ~2900, 1650 and strong band at 1092, 680 cm^{-1} which correspond to the –CH stretching, –OH bending, –C–O–C pyranose ring and –CH deformation of the cellulose I structure of BC, respectively.[30] Upon close examination of the carbonyl stretch signatures of the PLA/OLLA-g-BC film bionanocomposites contained dual peak at 1747 cm^{-1} and 1755 cm^{-1}. However, the peak intensity at 1747 cm^{-1} decreased as the concentration of OLLA-g-BC was increased.[15]

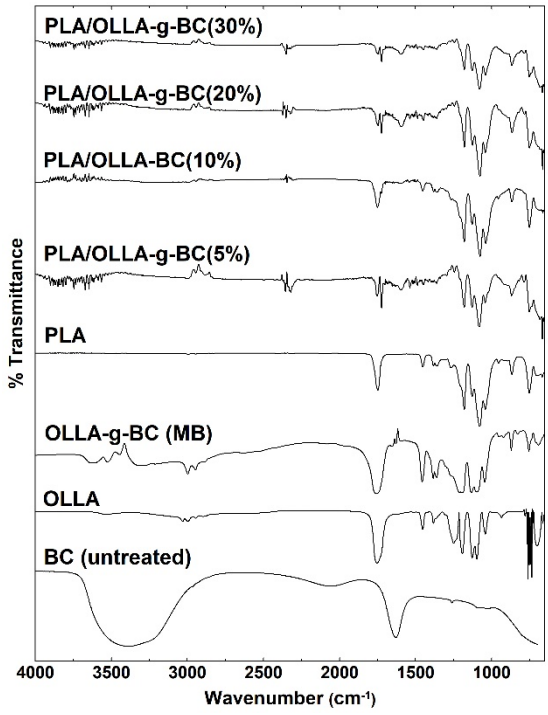

Figure 2: FTIR spectra for untreated BC, OLLA, OLLA-g-BC, PLA and PLA/OLLA-g-BC bionanocomposites.

Thermal analysis

Thermogravimetric analysis was performed on PLA and PLA/OLLA-g-BC bionanocomposites under inert nitrogen gas flow which are shown in Figure 3a. From the derivative thermograms (DTG) shown in Figure 3b, it can clearly be observed that all formulations show two peaks, first small peak in the temperature range 70-170 °C suggests the event of unbound moisture

being removed. The second mass loss event in PLA occurs in the temperature ranges 259-378 °C. For bionanocomposite films, this mass loss occurs at lower temperatures which affects thermal stability due to the presence of lower molecular weight oligomers. The onset of degradation temperatures for PLA, PLA/OLLA-g-BC (5%), PLA/OLLA-g-BC (10%), PLA/OLLA-g-BC (20%) and PLA/OLLA-g-BC (30%) are 250, 231, 219, 198 and 183 °C, respectively. The maximum degradation temperature (T_{max}) for PLA, PLA/OLLA-g-BC (5%), PLA/OLLA-g-BC (10%), PLA/OLLA-g-BC (20%) and PLA/OLLA-g-BC (30%) are 353, 368, 354, 350 and 347 °C, respectively. It is noteworthy to mention that all bionanocomposite films have a degradation temperature above 300 °C which is well above the PLA processing temperature. The corresponding percentage weight loss at T_{max} for PLA, PLA/OLLA-g-BC (5%), PLA/OLLA-g-BC (10%), PLA/OLLA-g-BC (20%) and PLA/OLLA-g-BC (30%) are 69, 70, 74, 75 and 80%, respectively. It can be observed that weight loss is higher in bionanocomposite films as compared to pristine PLA which is due to the presence of shorter chain, low molecular weight OLLA-g-BC in PLA matrix that reduces thermal stability.

DSC investigation was carried out to evaluate effect of incorporation of OLLA-g-BC on melting and crystalliation behaviour of PLA. Figure 3c shows the comparison between the second heating thermographs for all the formulations. The glass transition temperature (T_g) of PLA, PLA/OLLA-g-BC (5%), PLA/OLLA-g-BC (10%), PLA/OLLA-g-BC (20%) and PLA/OLLA-g-BC (30%) were found to be 59.7, 57.8, 55.8, 46.2 and 42.2 °C, respectively. It can be noticed that as the filler concentration is increased the T_g showed further reduction as high as a ~18 °C decrease upon 30% filler loading. The reduction in T_g can be explained by the existence of short-chained, low molecular weight OLLA species which can move freely unlike higher molecular weight PLA chains yielding a plasticization effect thus increasing the free volume. Appearance of a single T_g in all bionanocomposite films confirm a better compatibility of OLLA-g-BC with poly(lactic acid). The cold crystallization temperature (T_{cc}) for polylactide was witnessed at 97.1 °C, at lower loadings of OLLA-g-BC i.e. 5 and 10% the T_{cc} was not affected but upon increasing the loading to 20% the T_{cc} reduced to 93.6 °C which is due to the presence of deformed crystals in PLA.

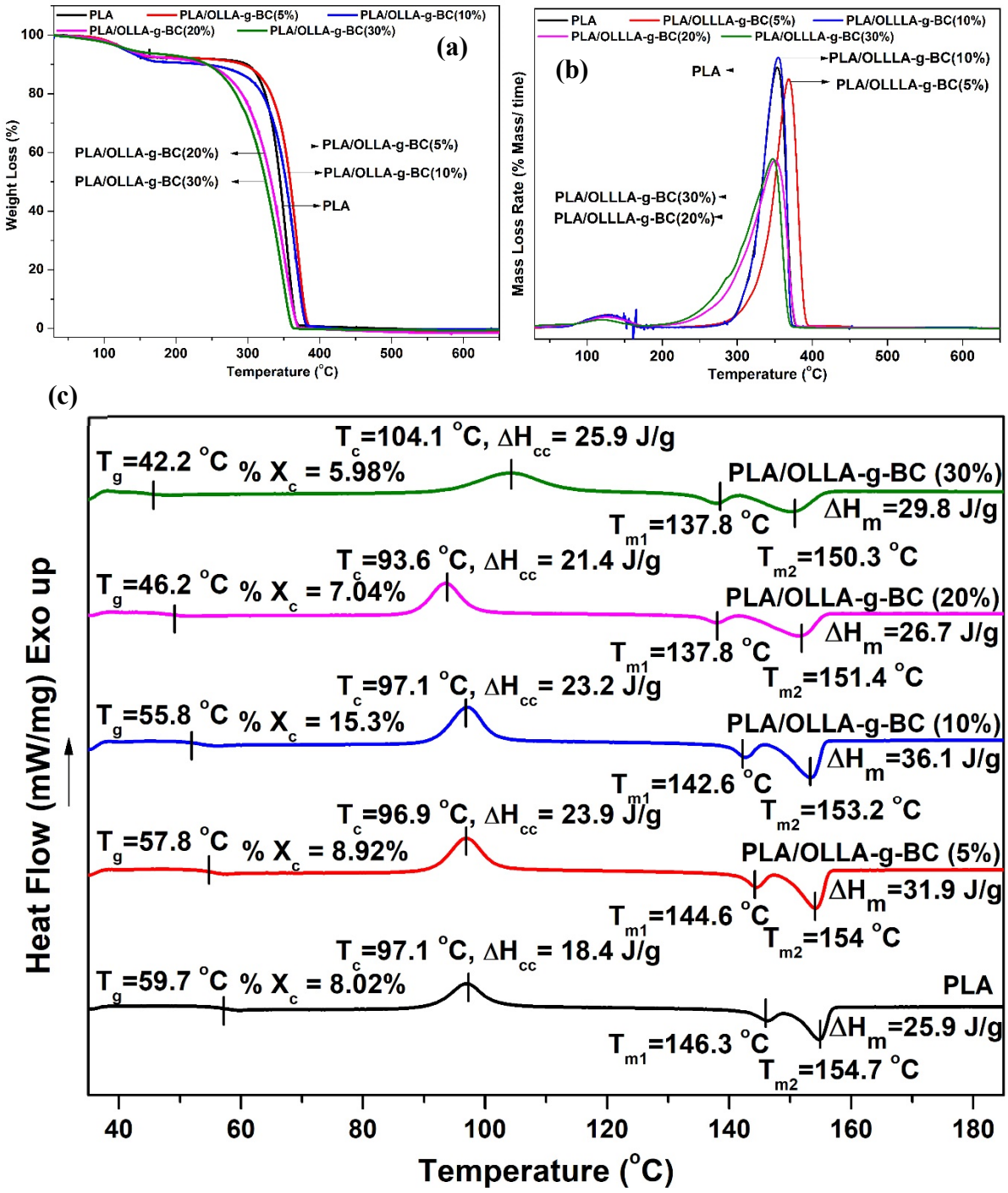

Figure 3: (a) TGA (b) DTG and (c) DSC thermograms for PLA and PLA/OLLA-g-BC bionanocomposite films.

When the loading was further increased to 30% the T_{cc} increased to 104.1 °C, this increase could possibly be due to the formation of agglomerates which delay the crystallization process. The endothermic phenomenon showed bimodal peaks for every formulation which denote the presence of α and β phase of PLA. The peak observed at lower temperature designates to the β-phase or the orthorhombic phase composed of thin imperfect whereas the peak appearing at

higher temperatures describes the α-phase or the pseudo-orthorhombic phase made up of perfect crystals.[31] The melting temperature (T_m) for PLA, PLA/OLLA-g-BC (5%), PLA/OLLA-g-BC (10%), PLA/OLLA-g-BC (20%) and PLA/OLLA-g-BC (30%) was found to be 154.7, 154, 153.2, 151.4 and 150.3 °C, respectively. As the filler loading increased the endothermic peak showed a gradual shift towards lower temperatures, this reduction in T_m was due to the formation irregular and heterogeneous crystals formed in presence of filler. This can also indicate towards the reduced stability of PLA in presence of OLLA-g-BC filler.

Crystallization kinetics

The isoltermal crystallization kinetic studies for PLA and PLA/OLLA-g-BC bionanocomposite films were carried out using DSC and POM at 120 °C. The thermograms of all formulations were obtained during isothermal condition obtained by rapid cooling of polymer melt at 120 °C and the enthalpy of crystallization was plotted against time as shown in Figure 4a. It can be observed that crystallization behaviour can be altered by addition of fillers which can be seen as the gradual reduction in half-time ($t_{0.5}$) as the filler loading is increased. It suggested that rate of crystallization is faster with increase in filler concentration. To develop more insight about the crystallization kinetics, the plots of crystallinity conversion (X_t) versus time were plotted as shown in Figure 4b. The isotherms obtained are sigmoidal in shape and the rate of crystallization for all bionanocomposites was lower than that of PLA. However, the curves shift gradually towards lower crystallization time indicating towards improvement in rate of crystallization with increasing filler loading. In addition, the Avrami equation was employed to plot $\ln[(-\ln(1-X_t))]$ against $\ln(t)$ for all formulations as depicted in Figure 4c. For comparison of Avrami profiles primary crystallization (X_t=30-70%) is considered i.e. region where a clear outward growth of lamellar stacks can be observed. The values of Avrami exponent (n) and rate constant (K) are tabulated in Table 1.

Surface morphology

The distribution and morphology of OLLA-g-BC filler into the PLA matrix was studied using FE-SEM and TEM techniques. Figure 5(a-d) shows the PLA and PLA/OLLA-g-BC bionanocomposites with increasing filler content. In all bionanocomposite film samples, untreated BC can be seen in form of nano-sized particles which are homogeneously dispersed throughout the matrix. However, in samples with higher concentration of fillers such as 30wt% (Figure 5d), showed agglomeration which reduced the homogeneity of the fracture surface giving rise to increased roughness. Average particle size for untreated BC nanoparticles in

PLA/OLLA-g-BC (5%), PLA/OLLA-g-BC (10%), PLA/OLLA-g-BC (20%) and PLA/OLLA-g-BC (30%) bionanocomposite films was 20.6±9.9, 18.8±10.8, 20.8±14.8 and 43.38±20.6 nm, respectively.

Transmission electron micrographs of PLA/OLLA-g-BC (30%) sample is shown in Figure 5e. It can be observed that untreated BC nanoparticles are homogeneously dispersed in the PLA matrix even at higher loadings. The average particle size of BC nano-spheres was found to be 61.8±16 nm with some evidence of agglomeration can also be observed which is depicted by arrows.

Molecular weight measurements

The molecular weight analysis was carried out to know the impact of addition of OLLA-g-BC in PLA matrix. The molecular weights of all formulations are listed in Table 2. The molecular weight analysis of masterbatch was carried out using gel permeation chromatography and the M_n and M_w were found out to be 0.6 and 0.8 kDa, respectively. At lower weight loadings of OLLA-g-BC such as 5 and 10 wt%, there is a minor reduction in number average molecular weight of 3.3 and 7.8%, respectively. As seen from Figure 6a, at higher weight loadings of 20 and 30 wt%, it was found that molecular weight distribution was bimodal unlike unimodal distribution as in case of lower oligomer concentrations which indicate the presence of lower molecular weight species in bionanocomposite films. The higher molecular weight products elute at low outflow time whereas low molecular weight products are detected much later. The secondary peak contribution for 20 and 30wt% bionanocomposite film samples were 6 and 22%, respectively.

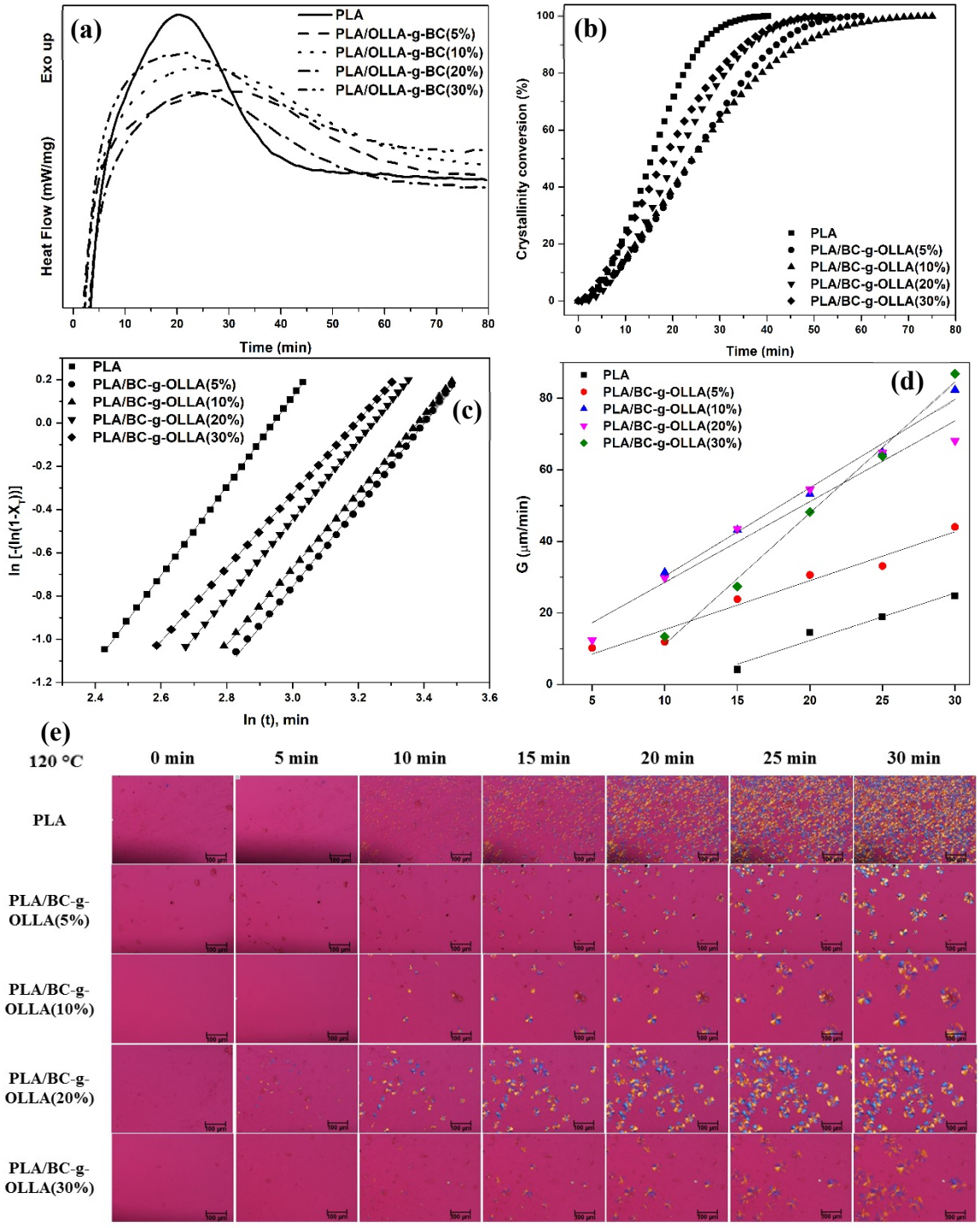

Figure 4: Plots of (a) heat flow vs. time, (b) relative crystallization vs. time, (c) Avrami curves, (d) growth rate of spherulites vs, isothermal hold time at 120 °C and (e) POM micrographs at different time intervals for PLA and PLA/OLLA-g-BC bionanocomposites.

Table 1: Thermal properties and crystallization kinetic data of PLA and PLA/OLLA-g-BC bionanocomposites.

Samples	T_{onset} (°C)	T_{max} (°C)	Wt_{losss} (%)	T_g (°C)	T_m (°C)	ΔH_m (J/g)	T_{cc} (°C)	ΔH_{cc} (J/g)	$\%X_c$	n	K $\times 10^{-3}$	$t_{0.5}^{exp}$	$t_{0.5}^{theo}$	N (num/um^2)	G
PLA	250	353	69	59.7	154.7	25.9	97.1	18.4	8.0	2.06	2.4	15.9	38.1	0.0012	1.33
PLA/OLLA-g-BC(5%)	231	368	70	57.8	154	31.9	96.9	23.9	8.9	1.88	1.7	24.6	46.5	0.00012	1.37
PLA/OLLA-g-BC(10%)	219	354	74	55.8	153.2	36.1	97.1	23.2	15.3	1.76	2.6	23.8	45.9	0.00003	2.47
PLA/OLLA-g-BC(20%)	198	350	75	46.2	151.4	26.7	93.6	21.4	7.0	1.82	2.7	20.9	43.7	0.00018	2.25
PLA/OLLA-g-BC(30%)	183	347	80	42.2	150.3	29.8	104.1	25.9	6.0	1.70	4.3	19.6	41.5	0.00006	3.67

T_{onset}: Onset of degradation temperature (°C); T_{max}: maximum degradation temperature (°C); Wt_{losss} (%): percentage weight Loss at maximum degradation temperature; T_g: Glass transition temperature (°C); T_m: Melting temperature (°C); ΔH_m: Heat Enthalpy of Fusion (J/g); T_{cc}: Cold Crystallization temperature (°C); ΔH_{cc}: Heat Enthalpy of crystallization (J/g); $\%X_c$: percentage crystallinity; n: Avrami exponent; K: crystallization rate constant, $t_{0.5}^{exp}$: experimental crystallization half-time; $t_{0.5}^{theo}$: theoretical crystallization half-time; N: density (No. of spherulites/μm^2); G: Spherulite Growth rate.

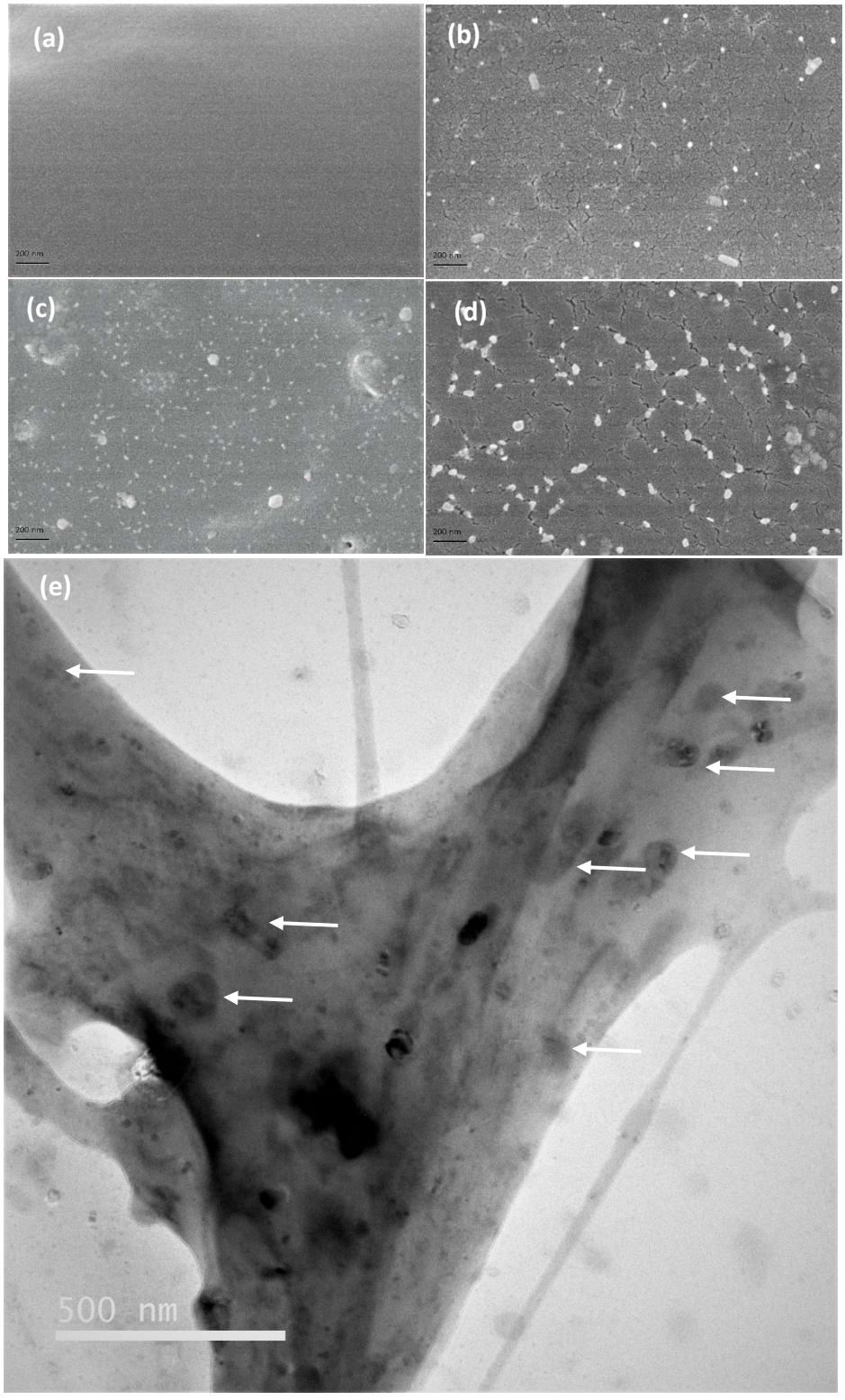

Figure 5: (a-d) FE-SEM micrographs of cryofractured sections of (a) PLA and PLA/OLLA-g-BC bionanocomposites (b) 5wt%, (c) 10wt%, (d) 30wt%; scale: 200nm and (e) TEM micrograph of PLA/OLLA-g-BC(20%) bionanocomposite; scale: 500 nm, white arrows depict BC nanospheres.

Table 2: Effect of filler loading (wt%) on molecular weight of PLA and PLA/OLLA-g-BC bionanocomposites.

Sample	**High intensity peak**			**Low intensity peak**		
	M_n (kDa)	**M_w (kDa)**	**PDI**	**M_n (kDa)**	**M_w (kDa)**	**PDI**
OLLA-g-BC	-	-	-	678±11.3	813±45.3	1.2±0.0
PLA	101.4±2.9	205.7±1.7	2.0±0.1	-	-	-
PLA/OLLA-g-BC(5%)	107.9±1.8	204.9±3.6	1.9±0.0	-	-	-
PLA/OLLA-g-BC(10%)	98.9±1.5	192.8±1.3	1.9±0.0	-	-	-
PLA/OLLA-g-BC(20%)	116.6±3.5	207.7±1.1	1.8±0.0	1.2±0.1	1.8±0.1	1.5±0.2
PLA/OLLA-g-BC(30%)	105.1±0.2	192.3±1.2	1.8±0.0	1.4±0.1	2.1±0.1	1.6±0.2

Mechanical Properties

The mechanical properties of PLA and PLA/OLLA-g-BC bionanocomposites were analysed and ultimate tensile strength, UTS (MPa), Young's modulus, E (MPa) and percentage elongation at break (%E) are shown in Figure 6b. The UTS, E and %E at break for PLA films were found to be 16.6±1.1 MPa, 3.3±0.6 MPa and 81.5±5.0%, respectively which matched closely with those reported by Zakaria, Islam, Hassan, Mohamad Haafiz, Arjmandi, Inuwa and Hasan [32]. It was observed that increasing the filler loading reduced the tensile strength of bionanocomposite films. With incorporation of 30wt% of filler the UTS showed a decrease of ~42% decrease. The short-chained OLLA oligomers align faster along the direction of load as compared to longer PLA chains which explains the reduction in UTS as the filler concentration was increased. The presence of short-chained OLLA oligomers give rise to increased free volume which resulted into poor interaction between OLLA-g-BC and PLA matrix thus reducing the chain entanglement effect.[3,15]. Young's modulus shows a gradual decrease as the filler loading is increased. At 20wt% loading the modulus showed a decrease of ~33% from 5.14±0.9 to 3.43±0.4 which indicates a decrease in stiffness and improvement in dispersion of filler.[3] Incorporation of short-chained OLLA increase the free volume which results in reduction in stiffness and increase in flexibility ~20%. However, upon further increasing the filler loading the free volume increased drastically resulting in phase separation between the oligomer and polymer matrix which resulted in gradual decrease in flexibility.

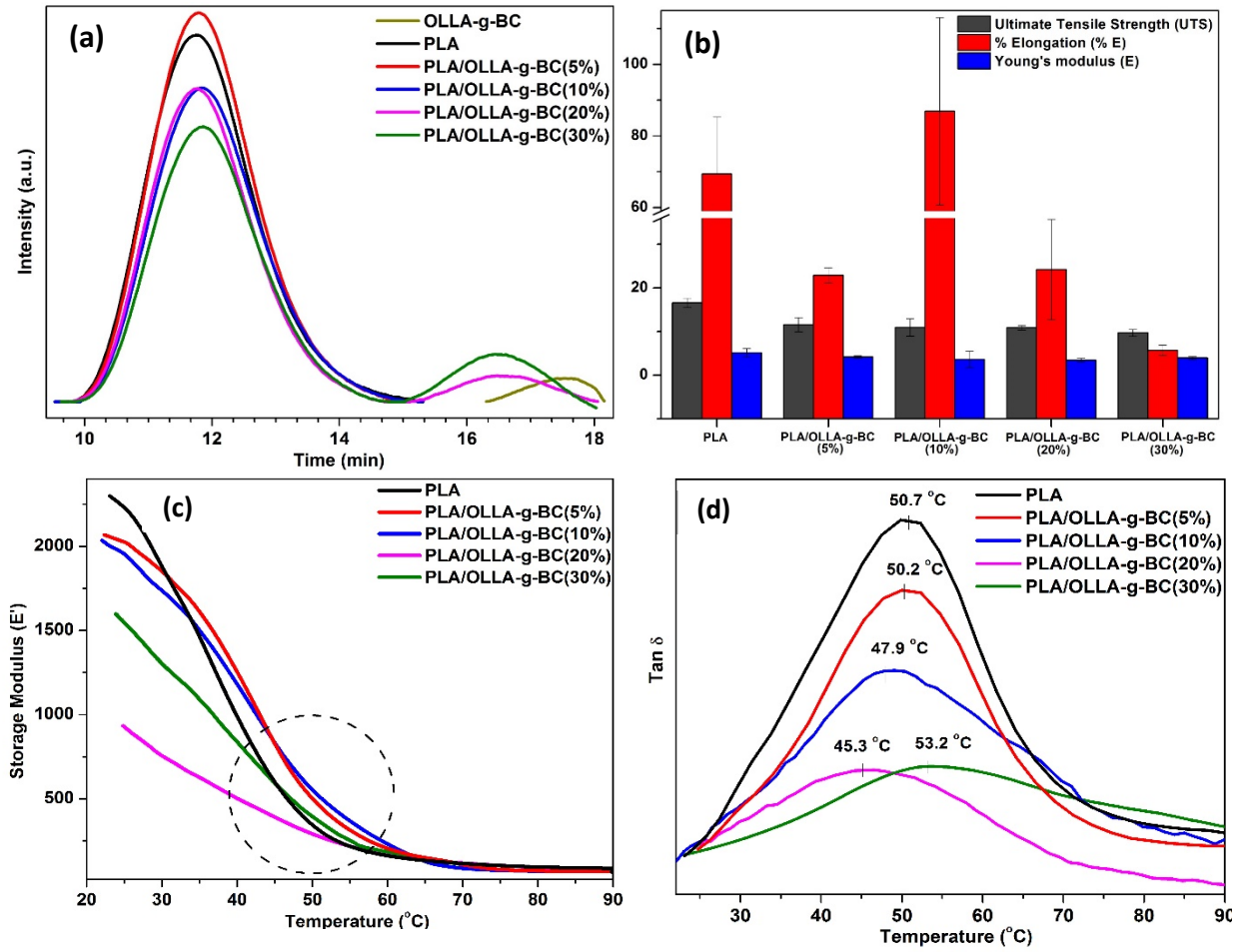

Figure 6: (a) Molecular weight intensity curves as a function of retention time, (b) Variation in mechanical properties, (c) storage modulus (E´) as a function of time and (d) tan δ as a function of time with increasing filler loading (wt%).

Thermomechanical studies

Thermomechanical tests are an important characterization to know the effect of addition of OLLA-g-BC filler on PLA which provides information about the dynamic properties of the formulations. PLA showed storage modulus value of 2306 MPa at 25 °C which showed a decrement of approximately 59% upon 20wt% filler loading as depicted in Figure 6c. This major reduction was due to two reasons firstly, the incorporation of OLLA-g-BC fillers which are short-chained oligomers, creating a plasticization effect and secondly, higher loading leads to agglomeration which inhibits the stress transfer between the filler and polymer matrix. These reasons ultimately affect the load-bearing capacity of composites i.e. storage modulus values. The E' values show an intense fall around 40-60 °C, depicted by a circle in Figure 6c which is also the glass transition temperature of PLA based bionanocomposites. The maxima of the tan

δ plot can be considered as the T_g of the polymer. PLA showed the peak at 50.7 °C which reduced gradually to 45.3 °C upon addition of 20 wt% OLLA filler plasticization effect as shown in Figure 6d. These results indicate improvement in impact resistance and elongation properties in PLA/OLLA-g-BC bionanocomposite which are key requirement for PLA based flexi-packaging.

Transparency and Color studies

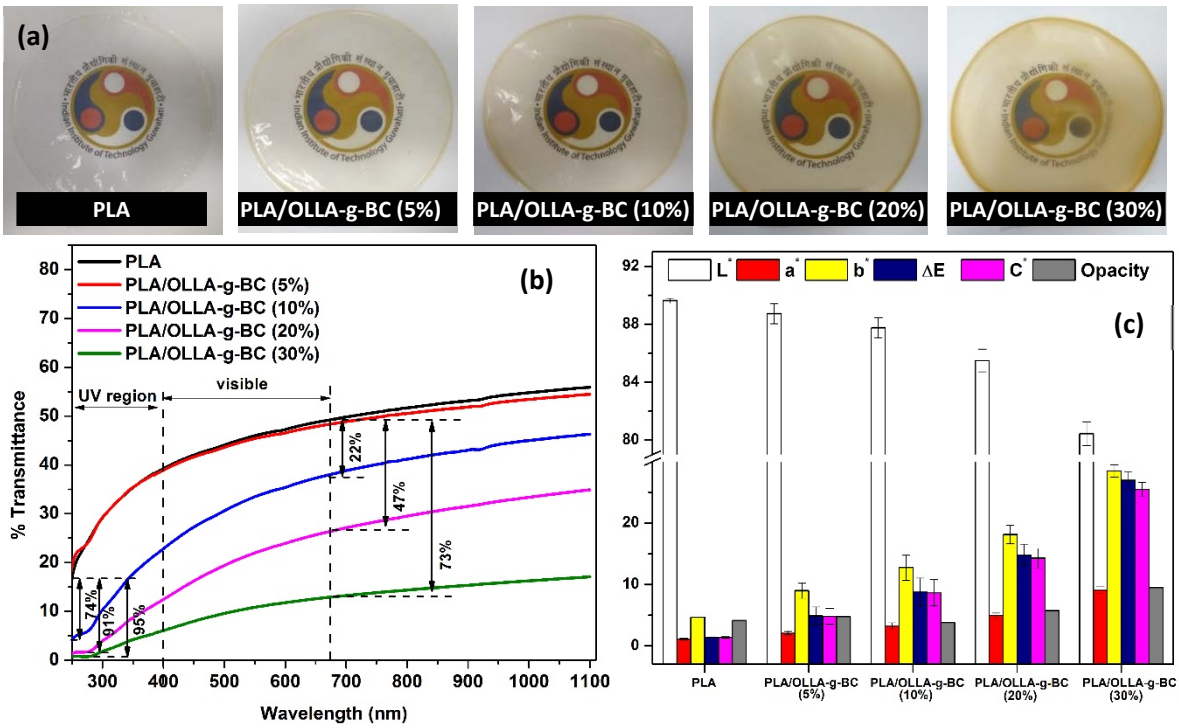

Figure 7: (a) Pictorial representation, (b) variation in transparency in the wavelength range 200-1100nm and (c) color parameters and opacity values of PLA and PLA/OLLA-g-BC bionanocomposite films.

The transparency and UV resistance have become vital to flexible packaging both on aesthetic and freshness point of view. PLA suffers from poor UV resistance which should be enhanced for its suitability in diverse uses. UV-visible examination was carried out for different formulations to determine the transparency of films as shown in Figure 7b. PLA percentage transmission values for ultra-violet region (400nm) and visible region (700nm) were 39.3 and 49.8%, respectively which are similar to the values reported earlier.[33] The transparency of PLA films depends strongly on the solvent type and processing methods such as solvent casting, extrusion or compression molding, etc. PLA shows an opacity values of 4.1 at 600nm which does not change much upon 5wt% filler loading. However, upon further loading the opacity

increases drastically for 20wt% and 30wt% having values of 5.7 and 9.5, respectively. The increase in opacity with increasing filler concentration is concurrent with the decrease in percentage transmittance as shown in Figure 7b. This increased opacity in bionanocomposite films was due to two reasons: firstly, due to the brown color given by the OLLA-g-BC filler and secondly due to the homogeneous dispersion of the nanofiller in the polymer matrix. Just like the visible region, similar trend of reduction in transparency can be noticed in UV region. For PLA, UV light is partially transmitted whereas remaining part is reflected by the PLA surface which acts as a mirror. At 250nm, the %T value for PLA bionanocomposite films reduced by 95% with incorporation of 30wt% filler which is because of the proper dispersion of OLLA-g-BC which acted as a UV blocking agent. Hence, PLA/OLLA-g-BC bionanocomposite can be a suitable candidate for packaging of UV sensitive food products.

The color parameters were altered upon inclusion of OLLA-g-BC fillers as can be seen in Figure 7c. The L*, a* and b* parameters obtained for PLA were 89.6±0.2, 1.1±0.1 and 4.7±0.03, respectively which were found concurrent with the values 89.8±0.2, -0.2225±0.0 and 4.614±0.2, respectively obtained by Patwa et al. [12]. It was found that the L* decreased while the a* and the b* values increased with the rise in filler loading. This suggests that the brown colored filler causes increase in darkness, redness and yellowness as seen from visual appearance of films. The color difference (E) and Chroma (C*) values increase from 1.4 and 1.4 to 27.0 and 25.5, respectively upon addition of 30wt% of filler which indicates the increase in saturation of colors.

Contact angle studies

The surface wetting characteristics of the PLA/OLLA-g-BC and bionanocomposite films was studied using the sessile drop contact angle measurements as shown in Figure 8a. The contact angle measured for PLA was around 83.5±0.8° which was found to be matching with the values reported elsewhere.[17] Due to the in-situ polymerization, condensation polymerization, the grafting process occurred where the polar (-OH) groups on BC backbone were replaced by hydrophobic ester groups of OLLA.[34] As a result of which, at low loadings of OLLA-g-BC fillers i.e. 5wt% and 10wt%, the contact angles were 102.5±1.7°, 85.4±1.7°, respectively. As evident from the SEM micrographs that at lower loadings the filler particles are thoroughly dispersed in the PLA matrix resulting in surface roughness which contributed to the such improvement in the hydrophobic character. Upon further increasing the filler concentration,

agglomeration of filler particles takes place which results in improper dispersion thus affecting the surface roughness and as a result of which the wettability of the films is similar to PLA.

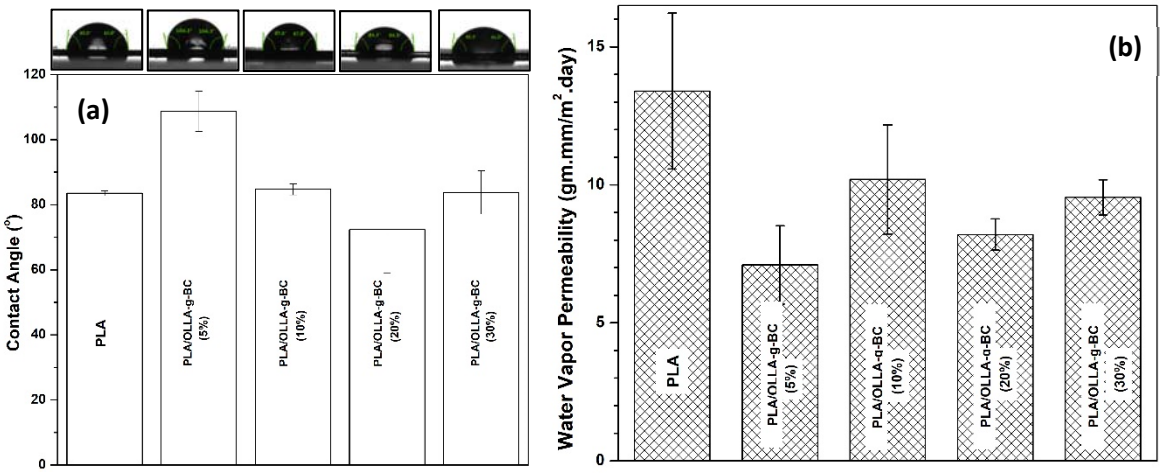

Figure 8: (a) contact angle variation with increasing filler loading (wt%) along with respective CCD image of drop and (b) variation in water vapour permeability of PLA and PLA/OLLA-g-BC bionanocomposite films.

Barrier Properties

Moisture and oxygen are the main culprits responsible for food degradation as they provide suitable environment for microbial growth. Hence, it is indispensible that a food packaging should have a low water vapor and oxygen permeability. Water vapor permeability for PLA films were 2.3±0.5 g.mm/m^2.day.kPa which was similar to Jamshidian et. Al [35]. In all formulations containing BC filler the water vapor values are lower than neat PLA. Upon addition of 10wt% BC filler the water vapor permeability was found to be lowest i.e. 1.3±0.2 g.mm/m^2.day.kPa which is around ~40% reduction. This significant reduction can be due to improved dispersion, hydrogen bonding between the OLLA-g-BC filler and PLA matrix. The water vapor permeability again increases with increasing filler concentration due to the agglomeration of fillers which affects proper dispersion.

Conclusions

In this work, PLA/OLLA-g-BC bionanocomposites were successfully prepared using solvent casting technique. Prior to that in-situ polycondensation polymerization reaction was done to disperse untreated BC within OLLA chains without any additive or catalyst. The PLA and PLA/OLLA-g-BC bionanocomposite films were manufactured by solvent evaporation method. The FTIR studies established that the grafting of OLLA chains on BC backbone occurred at –

OH functionality. through grafting between BC and OLLA as ascribed from the FTIR studies. The molecular weight of masterbatch (OLLA-g-BC) were found to be around 700 Da. FESEM micrographs show that untreated BC nanoparticles are homogeneously dispersed in PLA matrix whereas TEM images confirm the presence of nanospheres which suggests that addition of OLLA-g-BC significantly changes the morphology of bionanocomposite films. Both thermal analysis and mechanical testing studies revealed that incorporation of OLLA-g-BC induced plasticization which can be corroborated by decreased glass transition temperature and increased flexibility of bionanocomposites. Single glass transition temperature of PLA/OLLA-g-BC bionanocomposites at different filler concentration confirmed the compatibility of two materials. Untreated BC induced nucleating effect which decreased the crystallization temperatures and also lead to increasing of the fusion enthalpies. Furthermore, addition of OLLA-g-BC into PLA matrix lead to improved barrier properties due to tortuous path provided by homogeneously dispersed BC nanoparticles. DSC and POM analysis of bionanocomposite films showed that OLLA-g-BC can improve crystallization rate. The improvement in hydrophobicity was observed by contact angle analysis, which was due to the reduction in polar groups upon grafting. could improve mechanical and barrier properties of PLA films with suitable morphological, thermal and optical properties making it suitable for possible food packaging applications. To conclude, significant property improvements are obtained upon incorporation of untreated BC in PLA matrix, where both are obtained from natural bio resources which are abundant, non-toxic and truly fall in the class of "green" bioplastic for flexible food packaging applications.

Acknowledgements

This work was supported by Ministry of Education, Youth and Sports of the Czech Republic-Program NPU I (LO1504) and International Mobility of TBU researchers–CZ.02.2.69/0.0/0.0/16_027/0008464. Authors are also thankful to Dr. Oyunchimeg Zandraa, junior researcher at Tomas Bata University in Zlín, Czechia for providing the bacterial cellulose for this study. We would also like to acknowledge Centre of Excellence for Sustainable Polymers (CoE-SuSPol) supported by Department of Chemicals & Petrochemicals under the Ministry of Chemical & Fertilizers, Government of India and Central Instruments Facility (CIF) situated at Indian Institute of Technology Guwahati, India for allowing to use the available research facilities to carry out this research work.

References

1. Katiyar, V.; Nanavati, H., Polym. Eng. Sci. **2011**, 51, 2066.
2. Dhar, P.; Bhardwaj, U.; Kumar, A.; Katiyar, V. In Food Additives and Packaging; American Chemical Society, 2014, Chap. 17.
3. Pal, A. K.; Katiyar, V., Biomacromolecules **2016**, 17, 2603.
4. Gupta, A.; Katiyar, V., ACS Sustain. Chem. Eng. **2017**, 5, 6835.
5. Hakkarainen, M.; Karlsson, S.; Albertsson, A. C., Polymer **2000**, 41, 2331.
6. Ohkita, T.; Lee, S. H., J. Appl. Polym. Sci. **2006**, 100, 3009.
7. Ma, B.; Han, J.; Zhang, S.; Liu, F.; Wang, S.; Duan, J.; Sang, Y.; Jiang, H.; Li, D.; Ge, S., Acta Biomater. **2018**, 71, 108.
8. Pogorielov, M.; Hapchenko, A.; Deineka, V.; Rogulska, L.; Oleshko, O.; Vodseďálková, K.; Berezkinová, L.; Vysloužilová, L.; Klápšťová, A.; Erben, J., J. Biomed. Mater. Res. A. **2018**.
9. Tesfaye, M.; Patwa, R.; Gupta, A.; Kashyap, M. J.; Katiyar, V., Int. J. Biol. Macromol. **2017**, 101, 580.
10. Gupta, A.; Prasad, A.; Mulchandani, N.; Shah, M.; Ravi Sankar, M.; Kumar, S.; Katiyar, V., ACS Omega **2017**, 2, 4039.
11. Pivsa-Art, W.; Fujii, K.; Nomura, K.; Aso, Y.; Ohara, H.; Yamane, H., J Polym Sci. **2016**, 23, 144.
12. Patwa, R.; Kumar, A.; Katiyar, V., J. Appl. Polym. Sci. **2018**.
13. Dhar, P.; Gaur, S. S.; Soundararajan, N.; Gupta, A.; Bhasney, S. M.; Milli, M.; Kumar, A.; Katiyar, V., Ind. Eng. Chem. Res. **2017**, 56, 4718.
14. Pal, A. K.; Katiyar, V., Int. J. Biol. Macromol. **2017**, 95, 1267.
15. Tripathi, N.; Katiyar, V., J. Appl. Polym. Sci. **2016**, 133, n/a.
16. Patwa, R.; Singh, M.; Kumar, A.; Katiyar, V., Polym. Bull. **2018**, 1.
17. Chakraborty, G.; Gupta, A.; Pugazhenthi, G.; Katiyar, V., J. Appl. Polym. Sci. **2018**, 135, 46476.
18. Pour, Z. S.; Ghaemy, M., Compos. Sci. Technol. **2016**, 136, 145.
19. Thompson, J. A.; Chapman, K. W.; Koros, W. J.; Jones, C. W.; Nair, S., Microporous Mesoporous Mater. **2012**, 158, 292.
20. Park, C.; Ounaies, Z.; Watson, K. A.; Crooks, R. E.; Smith Jr, J.; Lowther, S. E.; Connell, J. W.; Siochi, E. J.; Harrison, J. S.; St Clair, T. L., Chem. Phys. Lett. **2002**, 364, 303.
21. Bandyoypadhyay, S.; Saha, N.; Brodnjak, U. V.; Saha, P., Mater. Res. Express **2018**, 5, 115405.

22. Ambrosio-Martín, J.; Fabra, M. J.; Lopez-Rubio, A.; Lagaron, J. M., Cellulose **2015**, 22, 1201.
23. Iguchi, M.; Yamanaka, S.; Budhiono, A., J. Mater. Res. **2000**, 35, 261.
24. Alonso, E.; Faria, M.; Mohammadkazemi, F.; Resnik, M.; Ferreira, A.; Cordeiro, N., Carbohydr. Polym. **2018**, 183, 254.
25. Chiulan, I.; Frone, A. N.; Panaitescu, D. M.; Nicolae, C. A.; Trusca, R., J. Appl. Polym. Sci. **2018**, 135, 45800.
26. Figueiredo, A. R. P.; Silvestre, A. J. D.; Neto, C. P.; Freire, C. S. R., Carbohydr. Polym. **2015**, 132, 400.
27. Lee, K.-Y.; Blaker, J. J.; Bismarck, A., Compos. Sci. Technol. **2009**, 69, 2724.
28. Patwa, R.; Kumar, A.; Katiyar, V., J. Appl. Polym. Sci. **2018**, 135, 46590.
29. Tripathi, N.; Katiyar, V., J. Appl. Polym. Sci. **2016**, 133.
30. Sriplai, N.; Mongkolthanaruk, W.; Eichhorn, S. J.; Pinitsoontorn, S., Carbohydr. Polym. **2018**, 192, 251.
31. Mustapa, I. R.; Shanks, R. A.; Kong, I., Asian Trans. Basic Appl. Sci. **2013**, 3, 29.
32. Zakaria, Z.; Islam, M.; Hassan, A.; Mohamad Haafiz, M. K.; Arjmandi, R.; Inuwa, I. M.; Hasan, M., Adv. Mater. Sci. Eng. **2013**, 2013.
33. Pal, A. K.; Bhattacharjee, S. K.; Gaur, S. S.; Pal, A.; Katiyar, V., J. Appl. Polym. Sci. **2018**, 135, 45546.
34. Tripathi, N.; Katiyar, V., Int. J. Biol. Macromol. **2018**, 120, 711.
35. Jamshidian, M.; Tehrany, E. A.; Imran, M.; Akhtar, M. J.; Cleymand, F.; Desobry, S., J. Food Eng. **2012**, 110, 380.